JOURNAL OF Applied Polymer SCIENCE

Synergistic effects of carbon nanotubes and carbon black on the fracture and fatigue resistance of natural rubber composites

Bin Dong,[1] Chang Liu,[1] Yonglai Lu,[1,2] Youping Wu[1,2]

[1]State Key Laboratory of Organic–Inorganic Composites, Beijing University of Chemical Technology, Beijing 100029, China
[2]Beijing Engineering Research Center of Advanced Elastomers, Beijing University of Chemical Technology, Beijing 100029, China
Correspondence to: Y. Wu (E-mail: wuyp@mail.buct.edu.cn)

ABSTRACT: The quasi-static fracture and dynamic fatigue behaviors of natural rubber composites reinforced with hybrid carbon nanotube bundles (CNTBs) and carbon black (CB) at similar hardness values were investigated on the basis of fracture mechanical methods. Mechanical measurement and *J*-integral tests were carried out to characterize the quasi-static fracture resistance. Dynamic fatigue tests were performed under cyclic constant strain conditions with single-edged notched test pieces. The results indicate that synergistic effects between CNTBs and CB on the mechanical properties, fracture, and fatigue resistance were obtained. The composite reinforced with 3-phr CNTBs displayed the strongest fatigue resistance. The synergistic mechanisms and dominating factors of quasi-static and dynamic failure, such as the dispersion state of nanotubes, hybrid filler network structure, strain-induced crystallization, tearing energy input, and viscoelastic hysteresis loss, were examined. The weakest fatigue resistance of the composite filled with 5-phr CNTBs was ascribed to its strikingly high hysteresis, which resulted in marked heat generation under dynamic fatigue conditions. © 2015 Wiley Periodicals, Inc. J. Appl. Polym. Sci. **2015**, *132*, 42075.

KEYWORDS: composites; graphene and fullerenes; mechanical properties; nanotubes; rubber

Received 19 November 2014; accepted 4 February 2015
DOI: 10.1002/app.42075

INTRODUCTION

Elastomers reinforced with different nanofillers are widely used in some applications, such as auto tire and conveyer belts, which are always exposed to cyclic deformation conditions. Under such conditions, microcracks may be initiated and then propagate from stress-concentration points; this eventually causes the total failure of the rubber products.[1,2] Therefore, the crack initiation and propagation resistance play important roles in practical applications. Many factors have been demonstrated to influence the fracture mechanical behaviors of rubbers; these include mechanical load history, environmental conditions, rubber formulation, and constitutive behaviors.[3] In rubber formulation, the rubber type and reinforced filler play decisive roles. Whether or not the adopted rubber exhibits strain-induced crystallization is the primary consideration. The shape factor, surface activity, dispersion state, and volume fraction of the reinforced filler, the interfacial interaction between the filler and rubber chains, and the filler–filler networking all highly influence the failure behaviors of rubber composites.

The concepts of fracture mechanics have been considered to be the fundamental theories for studying the fracture and fatigue behaviors of rubber materials.[4,5] Rivlin and Thomas[6] proposed the tearing energy (G) theory in 1953 on the basis of the Griffith criterion.[6] Studies demonstrated that the fatigue crack growth rate (da/dN) for certain elastomers could be uniquely determined by G.[7,8] Four distinct regimes of fatigue crack growth behavior based on the maximum G were found under cyclic strains with a zero R ratio (means the minimum strain amplitude divided by the maximum strain amplitude).[9] *J*-integral theory, another powerful fracture mechanical concept, was first proposed by Rice and Rosengren[10] in the field of metals and plastics. Researchers have developed the *J*-integral theory to evaluate the quasi-static fracture resistance of rubber composites.[11–14] The fracture behaviors of silica/carbon black (CB)/natural rubber (NR) composites were investigated on the basis of *J* testing by our research group.[15] The results reveal that the critical *J* value (J_{IC}) was dependent on the precut length and remained almost constant in a medium precut length range. The fatigue resistance of the silica/CB/NR composites could be predicted by J_{IC}, tearing modulus (T_R), and strain energy density (SED).

Recently, one-dimensional carbon nanotubes (CNTs) were shown to be an attractive nanofiller in polymer fields because of their

Additional Supporting Information may be found in the online version of this article.

unique combination of outstanding thermal conductivity, electrical conductivity, and mechanical reinforcing efficiency; this makes it an ideal candidate for the design of advanced materials.[16–22] Great efforts have been made to improve the mechanical, electrical, and thermal performances of CNT-reinforced elastomer composites.[16–19] Meanwhile, extensive attention has also been concentrated in the field of hybrid filler systems, where different kinds of fillers, such as CNTs and CB, have combined use in elastomers.[20–22] This revealed that CNTs and CB might exhibit possible synergistic effects on the mechanical, electrical, and thermal properties. However, the quasi-static fracture and dynamic fatigue behaviors, which were very significant for the application of rubber articles, has received only a little attention.[14,16,22] Agnelli *et al.*[14] assessed the fracture resistance of hydrogenated nitrile butadiene rubber (HNBR) composites reinforced with 30-phr multiwalled CNTs by *J* testing. Lorenz *et al.*[16] compared the dynamic crack growth properties of two different kinds of NR–silica (40 phr) composites with CNTs (3 phr) and without CNTs. This showed that *da*/*dN* of the NR–silica composite with 3-phr CNTs was smaller compared with the composite without CNTs below a *G* of about 3 N/mm. However, at higher *G*s, the NR–silica composite with 3-phr CNTs exhibited a higher *da*/*dN* than the composite without CNTs. Fritzsche *et al.*[22] investigated the fatigue resistance of NR composites reinforced with hybrid CNTs and silica with a total filler loading of 90 phr. The results suggested that the fatigue resistance of the CNTs samples was better than that of the samples without CNTs under small-strain conditions. However, the silica-filled samples without CNTs showed the best performance at higher tearing energies. Despite these, few efforts have been made to examine the failure mechanisms of CNT-reinforced rubber composites under quasi-static and dynamic conditions.

Therefore, the focus of this study was to understand the influence of the CNT partial replacement of CB on the fracture and fatigue behaviors of CB/NR composites. Composites with similar hardness levels were obtained by a mechanical blending method. The traditional mechanical properties, such as the tensile strength and tear strength, were used to measure the reinforcing efficiency of the hybrid CNTs and CB for NR composites. From the view of energy, *J*-integral testing was adopted to characterize the quasi-static fracture behaviors. J_{IC} and T_R were used to measure the resistance to crack initiation and propagation, respectively. Dynamic fatigue tests were carried out under constant-strain conditions with single-edged notched test (SENT) specimens. Fatigue *da*/*dN*s and fatigue lifetimes under varied strains were obtained. Synergistic effects on the mechanical performance, quasi-static fracture, and dynamic fatigue properties of the NR composites reinforced with hybrid CNTs and CB were realized. The results are discussed in detail from the aspects of the filler network, dispersion state of CNTs, strain-induced crystallization, *G* input, viscoelastic hysteresis loss, and so on. This exploratory work can be considered a beneficial basis for the great potential applications of CNTs in rubber fields.

EXPERIMENTAL

Materials

The formulas of the four composites are detailed in Table S1 (in the Supporting Information). We adopted a kind of easily dispersed, highly one-dimensional aligned carbon nanotube bundles (CNTBs) instead of traditional pristine CNTs with a highly entangled structure to prepare the rubber composites by a mechanical blending method.[23] Here, 1-phr CNTBs were used to partially replace 3-phr CB N234 to obtain the composites with similar hardness levels. The reason was that commercially, the alteration of a rubber formulation is usually made in such a way as to keep the hardness of the rubber products constant.[24] CNTB-0, CNTB-1, CNTB-3, and CNTB-5 indicate that the contents of CNTBs were 0, 1, 3, and 5 phr, respectively; meanwhile, the contents of N234 were 25, 22, 16, and 10 phr. NR was produced by Yunnan Rubber Products Co., Ltd. (China). CB N234 and N330 were purchased from Tianjin Cabot Chemical Products Co., Ltd. (China). CNTBs (FloTube TM 7000) were provided by Beijing CNano Technology, Ltd. (China), with a purity of 92%, length greater than 50 μm, and diameter of 6–8 nm. The other ingredients were commercially available industrial products.

Sample Preparation and Measurement

Sample Preparation. The CNTB/CB/NR compounds were prepared in a two-roll mill by a traditional mechanical compounding method. The vulcanization properties of the compounds, such as the optimum curing time, were determined by a moving die rheometer at 143°C. Compounds were then cured for optimum curing time in the form of 2 mm thick sheets at 143°C and 15 MPa.

Transmission Electron Microscopy (TEM). The dispersion state of CNTBs in the CB/NR matrix and its hybrid network structure between CNTBs and CB were investigated with a Tecnai G2 20 transmission electron microscope produced by FEI Co., Ltd. (Hong Kong). The ultrathin sections of the samples were prepared by a liquid-nitrogen-cooled microtome at −100°C.

Rubber Process Analysis. The strain amplitude dependence of the shear storage modulus (G') was measured by an RPA 2000 rheometer rubber process analyzer (Alpha Technologies Co.) at a temperature of 60°C and a frequency of 10 Hz. The strain amplitude was in the range from 0.27 to 40%. G' in the low-strain regime was related to the filler–filler network structure.

Mechanical Properties. The tensile and tear properties were measured with an electronic tensile machine (Shenzhen SANS Test Machine Co., Ltd., China) with a crosshead speed of 500 mm/min according to ISO 37: 2011 and ISO 34-1: 2010, respectively. In addition, the Shore A hardness was measured according to ISO 868: 2003.

***J*-Integral Tests.** *J* testing was performed on SENT specimens with different precut lengths and at a crosshead speed of 20 mm/min at room temperature. Precut specimens with a width of 15 mm, thickness of 2 mm, and working gauge length of 50 mm were adopted to measure *J* value according to the following equation:

$$J = -\left(\frac{\partial U}{\partial A}\right)_{\Delta} = -\frac{1}{B}\left(\frac{\partial U}{\partial a}\right)_{\Delta} \quad (1)$$

where *U* is the strain energy at a considered displacement Δ, *A* is the fracture surface area, and *B* and *a* are the specimen thickness and crack length, respectively.

The detailed process of J testing was described in our previous work.[15] Briefly, crack-tip opening displacement (CTOD) was considered an indirect reflection of crack advancement.[14] Certain CTOD was related to the corresponding J value, and then, a plot of J-CTOD was obtained. J_{IC} was defined as the J value when CTOD was equal to 0.1 mm and was regulated as the crack initiation point.[25] T_R, which reflected the quasi-static crack propagation resistance, was measured by the slope of the J–CTOD curve at the very beginning of fracture propagation, for example, in the CTOD range from 0.1 to 0.5 mm, as shown in eq. (2):[26]

$$T_R = \left.\frac{dJ}{d\mathrm{CTOD}}\right|_{\mathrm{CTOD}\in[0.1\mathrm{mm},\,0.5\mathrm{mm}]} \tag{2}$$

In our study, specimens with a precut length of 4 mm were used to measure the J_{IC} and T_R values. To easily determine the crack-initiation points during fracture processing, the crack tips of the SENT specimens were coated with silver powder before testing. A Canon EOS 70D camera was placed in front of the crack tip to monitor the CTOD within a fixed time intervals.

Dynamic Fatigue Tests. Fatigue tests with SENT specimens with precut lengths of 1 mm were performed with an MZ-4003B displacement-controlled machine in a laboratory atmosphere with a constant frequency of 5 Hz. The testing conditions included different strain amplitudes: 30, 50, 70, 80, 90, and 100%. Before the tests, uncracked specimens were subjected to 2000 cycles to lower the Mullins effect (stress-softening effect) and residual stretching, and precuts with a length of 1 mm were introduced into the edge of the rubber specimens with a sharp cutter. During the tests, the machine was stopped periodically to record a with a digital camera. Stable da/dN was measured by the linear slope of a versus the number of fatigue cycles (N) in the range of 1–2 mm.

The fatigue resistance of rubbers is usually characterized by the relationship between da/dN and G. The G can be considered as the driving force for crack propagation, and it is a fundamental property, which governs crack propagation in elastomers.[27] For the SENT specimen with a precut length a, G can be measured by the following equations:[1]

$$G = 2kwa = 2\frac{\pi}{\sqrt{1+\varepsilon}}wa \tag{3}$$

where the parameter k is a slowly varying function of strain (ε) and w is the strain energy density (also abbreviated as SED). An empirical power law relationship between a stable fatigue da/dN and G was described by Paris and Erdogan[28] in the following equation:

$$\frac{da}{dN} = BG^{\beta} \tag{4}$$

where B and β are material constants determined by the experiment. The exponent β reflects the sensitivity of da/dN with respect to the tear energy.

Dynamic Mechanical Thermal Analysis. The dynamic mechanical thermal characteristics of the composites were measured under tension mode with a VA3000 dynamic mechanical thermal analyzer produced by AREVA 01dB-Metravib (France) Co., Ltd. The specimens were 15 × 15 × 2 mm^3 and were stretched under a strain amplitude of a 0.1%, a frequency of 5 Hz, and a wide temperature range from −80 to 30°C. The storage modulus (E') and loss modulus (E'') of the composites under different temperatures were obtained.

SED and Hysteresis Energy Density (HED). Cyclic stress–strain curves were used to simulate the stress–strain behavior per cycle during the dynamic fatigue tests under different strain conditions. Before the test, the Mullins effect was first minimized. Two fundamental parameters, SED and HED, were obtained from the area under the retractive (unloading) curve and hysteresis loop area, respectively.

RESULTS AND DISCUSSION

Dispersion State of the CNTBs and Hybrid Filler Network

Generally, the dispersion state of fillers in a polymer matrix is one of the critical factors that determines the fracture mechanical properties of nanocomposites.[29] The dispersion morphology of the nanotubes and CB in the NR matrix was directly evaluated by TEM. Typical TEM graphs of the CNTB/CB/NR composites are shown in Figure 1. As expected, composites with a rather homogeneous distribution of nanotubes were obtained. TEM images also confirmed that the CB aggregates were bridged through the fibrous CNTBs to form a hybrid filler network. Homogeneous dispersion of the nanotubes and formed hybrid filler network could ensure an effective load transfer and additional energy dissipation during deformation; this contributed to the quasi-static and dynamic crack resistance of rubber composites.

The nonlinear viscoelastic behavior as a function of the strain was also investigated. Generally, the absolute value of G' in the low-strain regime indicates the degree of filler network or filler–filler interaction.[30] A large nonlinear reduction of E' with increasing strain, commonly known as the Payne effect, is presented in Figure 2. Payne effect was mainly caused by the partial breakdown of the filler–filler networks and debonding/slippage between molecular chains and the filler aggregates, all of which resulted in a softening of the rubber and additional energy dissipation when the strain amplitudes increased.[31] The magnitude of the Payne effect followed the following order: CNTB-5, CNTB-3, CNTB-0, and CNTB-1. It suggested that only when the composite was filled with 3-phr CNTBs or more than 3-phr CNTBs would a more powerful hybrid filler network be formed. However, with the lowest total filler loading, CNTB-5 exhibited the highest E' and magnitude of the Payne effect; this indicated the formation of a most powerful filler network; meanwhile, the strongest energy dissipation under deformation.

Mechanical Properties

The mechanical properties of the CNTB/CB/NR composites with similar shore A hardness (with maximum differences of only about 6%) are summarized in Table I. Remarkable increments in the stress at 100 and 300% were perceived, especially for the CNTB-5 composite, which showed an increment of about 64% in stress at 100% and a 57% increase in stress at 300%, compared with CNTB-0. The tensile strength and tear strength were also improved; this indicated an enhanced

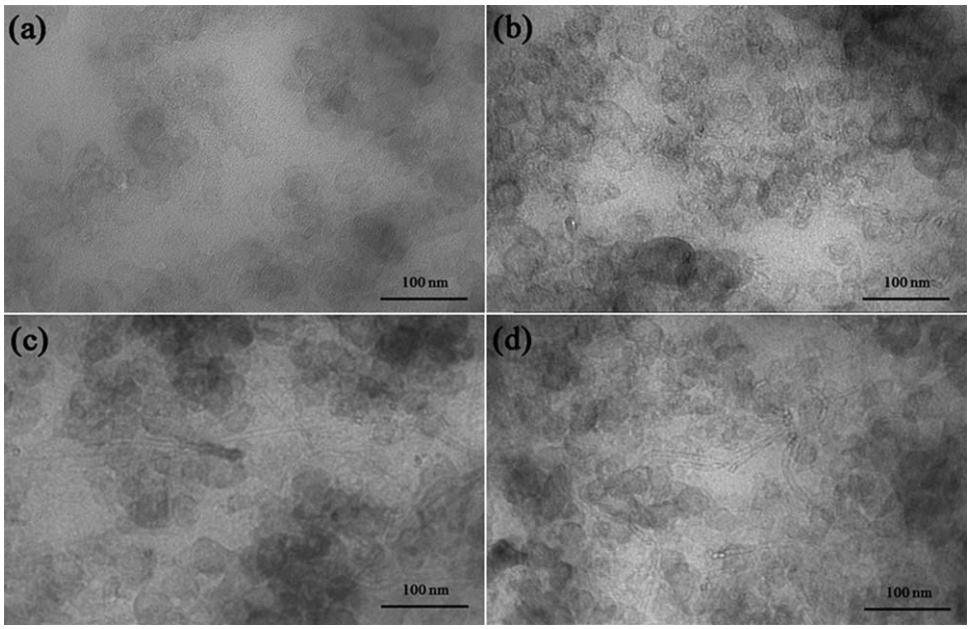

Figure 1. TEM micrographs of four different CNTB/CB/NR composites: (a) CNTB-0, (b) CNTB-1, (c) CNTB-3, and (d) CNTB-5.

fracture resistance with increasing content of CNTBs. An obviously higher reinforcing efficiency of fibroid CNTBs compared to spherical CB was also realized. We ascribed the powerful reinforcement of the CNTBs to their special one-dimensional structure with a strikingly high aspect ratio and specific surface area.

Questions arose from the fact that the tensile strength and tear strength were both controlled by the maximum load at break; namely, they only reflected the strength properties of rubbers.[4] Gent[32] showed that because of the randomness of flaws or microcracks that naturally existed or were introduced, the variations in the form of the crack propagation behaviors for different rubber materials and tensile strength could not be considered a useful indicator or criterion for quasi-static fracture performance. Reincke *et al.*[4] pointed out that the tear strength could deliver the wrong result when the crack toughness behavior was determined only by the deformation. Fracture mechanical tests, such as *J*-integral tests, where the load and deformation were both taken into account, could react sensitively to the structural changes of the materials from an energetic perspective.[4,5]

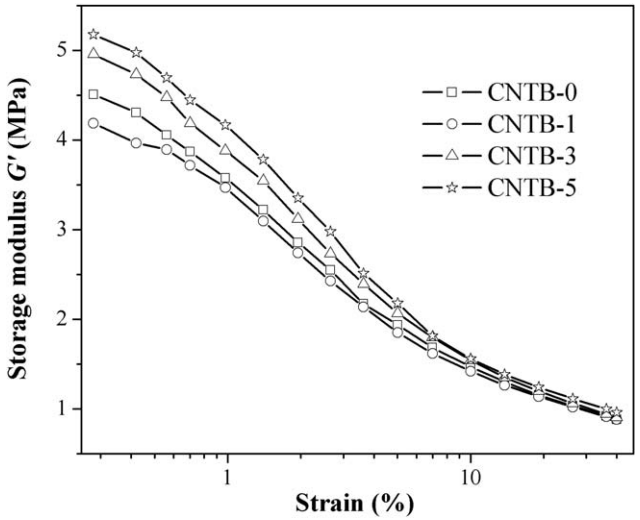

Figure 2. G' versus dynamic strain amplitudes.

Quasi-Static Fracture Resistance by *J*-Testing

J-integral tests are powerful methods for measuring the quasi-static crack initiation and propagation resistance of rubbers.[26] Plots of the *J* value versus CTOD of the four composites with a precut length of 4 mm are shown in Figure 3. J_{IC} was used to characterize the crack initiation resistance; T_R, a parameter indicating the crack propagation resistance, was measured by the linear slope of the *J* value versus CTOD curves. The corresponding J_{IC}, T_R, and the correlation coefficient (R^2) values of the four composites at a precut length of 4 mm are shown in Table II.

Comparing the values summarized in Table II, we noted that CNTB-5 had the highest values of J_{IC} and T_R; this indicated the strongest resistance to crack initiation and propagation; this was followed by CNTB-3 and CNTB-1. The NR composite filled with pure CB exhibited the weakest fracture resistance. From the results based on *J*-integral testing, we made sure that the CNTB partial replacement of CB indeed enhanced the quasi-static fracture resistance, including both the crack initiation and propagation performance.

Dynamic Fatigue Resistance

The dynamic fatigue properties of the four composites were performed with SENT specimens in a broad strain range. A representative example of fatigue crack growth curves under a strain of 70% is shown in Figure 4. Fatigue crack growth curves under other strains followed a similar tendency. During the very beginning of the process, the crack growth behavior could be considered a stable growth process (e.g., in an *a* range of

Table I. Mechanical Properties of Different Rubber Composites

Sample	Stress at 100% (MPa)	Stress at 300% (MPa)	Tensile strength (MPa)	Elongation at break (%)	Tear strength (kN/m)	Shore A hardness
CNTB-0	2.2	8.7	24.9	659	91.8	71
CNTB-1	2.5	9.9	25.9	640	99.8	73
CNTB-3	2.7	11.2	26.5	620	103.0	74
CNTB-5	3.6	13.7	28.2	596	110.8	75

1–2 mm). Beyond this range, cracks grew unstably and failed rapidly. The *da*/*dN* values were all measured by the linear slope of *a* versus *N* in the range of 1–2 mm.

The fatigue lifetimes of the four composites at different strains are shown in Figure S1 (in the Supporting Information). It was noted that CNTB-3 exhibited the longest lifetime at any strain investigated; this was followed by CNTB-1 and CNTB-0 and indicated that CNTB-3 had the strongest resistance to fatigue crack growth. However, the fatigue lifetimes of CNTB-5 were shorter than those of the other composites, especially under large strains. This was opposite to the results obtained from mechanical and *J*-integral measurement. The reasons are discussed in detail in the following sections.

The *da*/*dN* values of the CNTB/CB/NR composites under different strains were plotted against *G* with a double-log scale, as presented in Figure 5. It was interesting to note that all of the composites were well fitted with a power law dependency over the whole range of *G* investigated. The fatigue parameters *B* and β were determined from eq. (4) and are listed in Table III. For a given *G*, CNTB-3 exhibited the lowest *da*/*dN* and exponent β, and this denoted the most powerful fatigue resistance. CNTB-5 owned the highest *da*/*dN* and exponent β, and this indicated the weakest fatigue resistance.

Strain-Induced Crystallization

Stress–strain plots of the CNTB/CB/NR composites were adopted to characterize the strain-induced crystallization. For crystalline rubbers, the upturn or steep increase in the stress–strain plot was attributed to two effects: limited extensibility of rubber chains and strain-induced crystallization.[33,34] The original double-parameter Mooney–Rivlin model could not separate these two effects. Furukawa *et al.*[33] proposed a modified factor [$f(\lambda)$] to eliminate the effect of the limited extensibility of rubber chains, as shown in eqs. (5) and (6):

$$\sigma = 2\left(C_1 + \frac{C_2}{\lambda}\right)\left(\lambda - \frac{1}{\lambda^2}\right) f(\lambda) \tag{5}$$

$$f(\lambda) \cong \left(1 + \frac{1}{3}\frac{\lambda^2}{\lambda_m^2}\right) \tag{6}$$

where σ is the nominal stress, λ is the extension ratio, λ_m is the maximum extension ratio at break point, and C_1 and C_2 are the Mooney–Rivlin constants. Here, the expression $(\lambda - \lambda^{-2})f(\lambda)$ is simplified as $F(\lambda)$. According to the modified Mooney–Rivlin equation, the plot of $\sigma/F(\lambda)$ as a function of the reciprocal of the extension ratio (λ^{-1}) should yield a linear region, from which the constant values of C_1 (intercept) and C_2 (slope) can be obtained. On the basis of the theory of Furukawa *et al.*,[33] the critical upturn extension ratio (λ_{up}) at which the strain-induced crystallization starts to appear can be calculated by the following equation:

$$\lambda_{up}^3 = \frac{3\lambda_m^2 C_2}{2C_1} \tag{7}$$

The plots of $\sigma/F(\lambda)$ versus λ^{-1} of the CNTB/CB/NR composites are presented in Figure S2 (in the Supporting Information), and the obtained values of C_1, C_2, and critical λ_{up} are listed in Table IV. Compared with the other composites, CNTB-5 displayed the largest value of C_1, which was dependent on the elastic modulus and crosslinking density. At lower λ^{-1}, a large and abrupt decline could be discerned for all of the composites. CNTB-5 owned the lowest value of λ_{up}; this demonstrated that the strain-induced crystallization of the NR composites was enhanced by the inclusion of CNTBs. This was mainly due to two reasons. One was that fibrous nanotubes with high anisotropy ratio could easily orient along the deformation direction.[35]

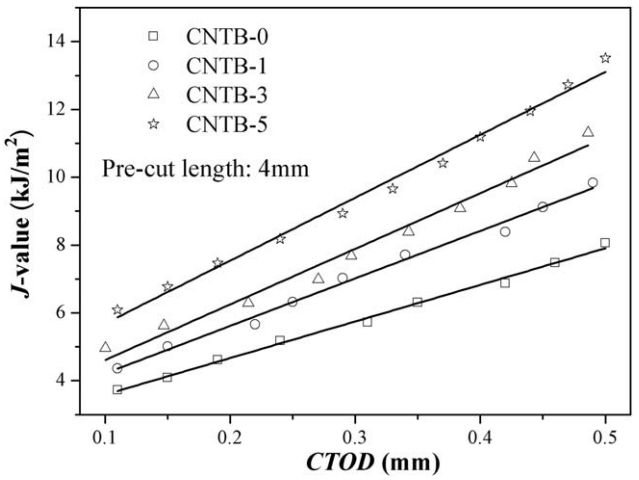

Figure 3. *J*–CTOD curves of four composites with a precut length of 4 mm.

Table II. J_{IC} and T_R Values of Four Composites at a Precut Length of 4 mm

Sample	J_{IC} (kJ/m²)	T_R (MPa)	R^2
CNTB-0	3.72	10.68	0.98
CNTB-1	4.36	14.02	0.99
CNTB-3	4.96	16.40	0.98
CNTB-5	6.09	18.23	0.99

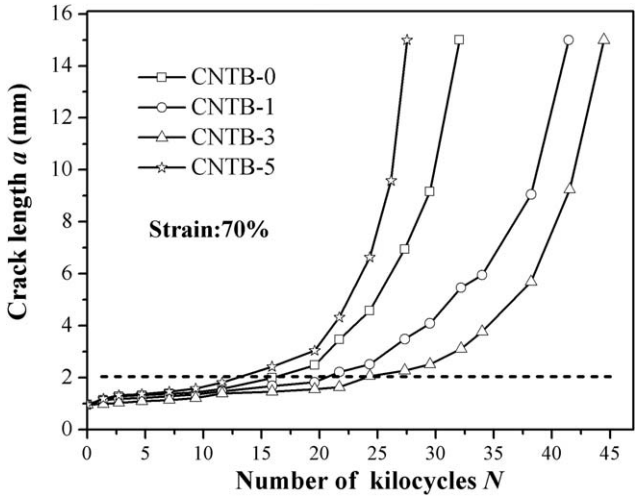

Figure 4. *a* versus *N* of the four composites at 70% strain.

The orientation of the CNTBs reduced the chain conformational entropy of this mixed system and induced the early orientation and crystallization of the rubber chains.[36] The other reason for the promotion of the strain-induced crystallization might have been the greater strain amplification near the crack tip induced by fibrous CNTBs compared to that of the spherical CB. This was confirmed by methods of digital image correlation and finite element analysis.[37,38] The oriented alignment of the rubber chains and CNTBs near the crack tip strongly enhanced crack deviation, blunting, and branching.[39] Typical graphs of fractured samples tested at 70% strain are presented in Figure 6. We noticed that the deviational tendency of the cracks was gradually enhanced with increasing CNTB content; this indicated increased crack growth resistance.

G Input

G directly dominates the fatigue crack growth resistance and fatigue life of rubbers.[3] According to eq. (3), for a SENT specimen with a certain *a* under a certain strain, *G* is proportional to SED. The SED values of the different composites under various strains are presented in Figure 7. Compared with the other composites, we noted that CNTB-5 possessed the highest SED by a slight margin under any strain. However, the differences among SED values under a certain strain were very small. For example, only a difference of about 9% at 100% strain between CNTB-0 and CNTB-5 was perceived. Here, we considered that there was similar *G* input per cycle with the increased CNTB content under a certain strain; this indicated that the driving forces for fatigue crack growth were almost equal. Therefore, the influence of energy input on the fatigue crack growth resistance could be ignored.

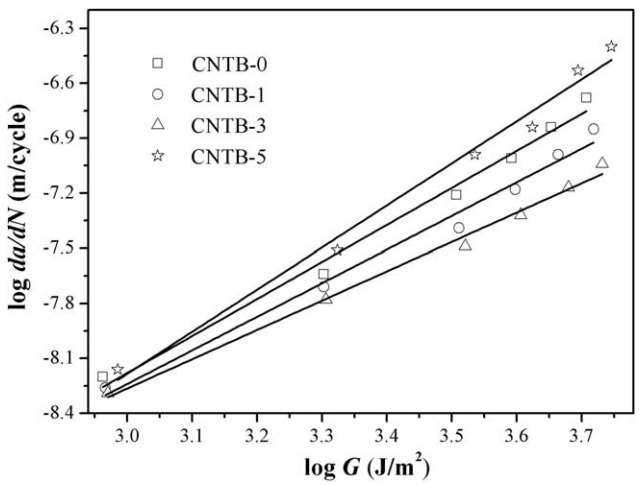

Figure 5. *da*/*dN* as a function of *G* for different composites.

Table III. Fatigue Parameters and R^2 Values of the Rubber Composites

Sample	*B*	β	R^2
CNTB-0	5.9×10^{-15}	2.02	0.98
CNTB-1	2.0×10^{-14}	1.83	0.98
CNTB-3	8.9×10^{-14}	1.59	0.99
CNTB-5	8.7×10^{-16}	2.29	0.97

Hysteresis Loss in the Bulk and at the Crack Tip

The energy dissipated in elastomers mainly has two contributions. The first is to the energy necessary for crack growth, and the second is ascribed to the viscoelastic dissipation, mostly the hysteresis loss.[40] Hysteresis describes the energy loss for internal friction contribution, which will be transformed into heat and can be largely affected by the inclusion of reinforced fillers.[41,42] Relationships between the hysteresis and crack growth resistance have been studied by many researchers.[43–45] Payne and Whittaker[43] proposed an expression that denoted that the hysteresis could improve the fracture energy, namely, the fracture resistance. Generally, in the cyclic fatigue process, moderate hysteresis could reduce the energy available to be released by crack growth and then enhance the fatigue resistance. However, a higher hysteresis might be detrimental to the fatigue properties under given dynamic conditions. The elevated temperature due to heat buildup could accelerate the rupture of the molecular chain and suppress the strain-induced crystallization for crystalline rubber, such as NR, all of which could weaken the fatigue resistance of rubber materials.[46] For quasi-static fracture, failure would occur in only one uniaxial stretch process; of course, heat generation should be ignored.

HED, a parameter characterizing the hysteresis loss in the bulk of composites, could be directly measured by the loop area of the cyclic stress–strain curves. The HED values of the CNTB/CB/NR composites under different strains are shown in Figure 8. Although the CNTB-5 composite was filled with the lowest

Table IV. Values of C_1, C_2, and λ_{up} Obtained from Modified Mooney–Rivlin Plots

Sample	C_1 (MPa)	C_2 (MPa)	λ_{up}
CNTB-0	0.371	0.402	4.54
CNTB-1	0.453	0.409	4.20
CNTB-3	0.627	0.453	3.83
CNTB-5	0.736	0.427	3.48

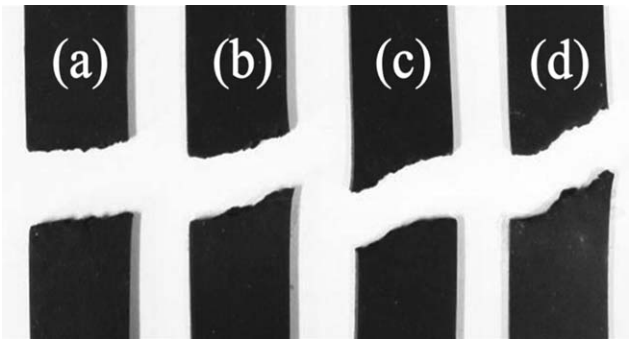

Figure 6. Graphs of fatigued samples tested at 70% strain: (a) CNTB-0, (b) CNTB-1, (c) CNTB-3, and (d) CNTB-5.

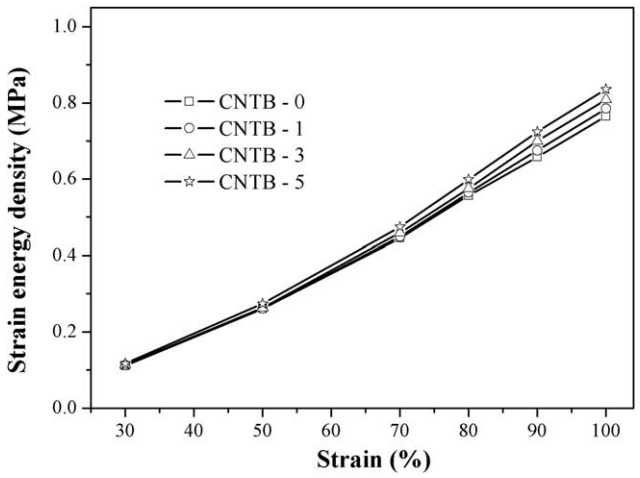

Figure 7. SED values of the CNTB/CB/NR composites under various strains.

content of fillers, it owned the highest HED by an extreme manner, especially under large strains. On the basis of the theory proposed by Persson and Brener,[40] the tearing energy $[G(v)]$ at a certain crack growth velocity (v) near the crack tip can be expressed as by the following equation:

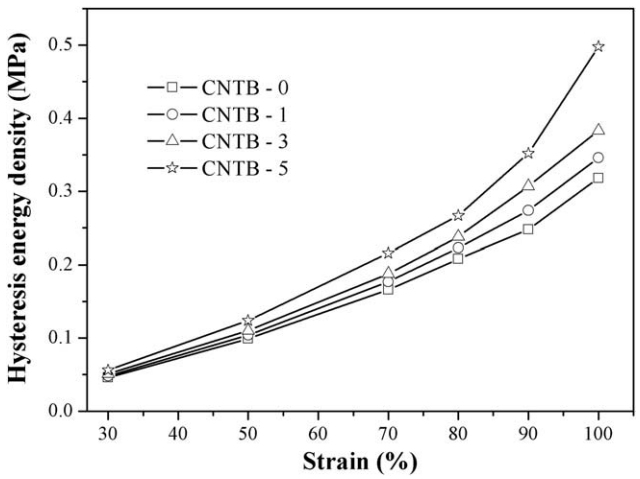

Figure 8. HED values of the CNTB/CB/NR composites under various strains.

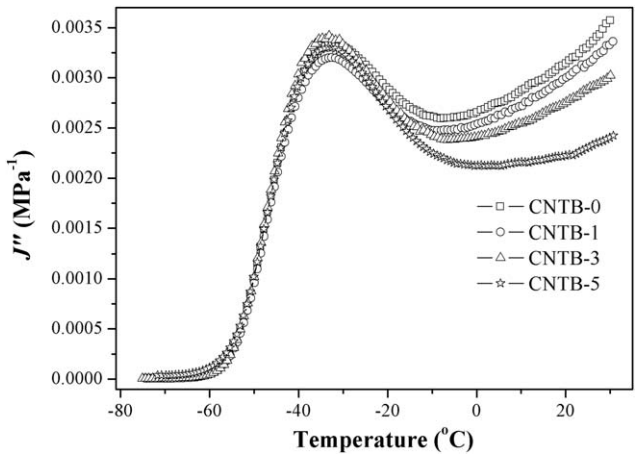

Figure 9. Dependence of J'' on the temperature for the CNTB/CB/NR composites.

$$G(v)=G_0\left[1+\frac{2}{\pi}E_0\int_0^{2\pi v/a}d\omega\frac{F(\omega)}{\omega}J''\right]^{-1} \quad (8)$$

where G_0 is the threshold energy to crack growth at the crack tip and $F(\omega)$ is a function of the frequency (ω), crack-tip diameter (a), and crack velocity (v). J'', a viscoelastic parameter termed *loss compliance*,[47] could be measured by E' and E'' according to eq. (9):

$$J''=\frac{E''}{E'^2+E''^2} \quad (9)$$

On the basis of the methods adopted by Nie *et al.* and Rooj *et al.*,[41,42] $G(v)$ at the crack tip during dynamic loading could be indirectly drawn from the measured temperature-sweep data of DMTA. Equation (8) revealed that a composite with a lower J'' corresponded to a higher value of $G(v)$; this indicated a higher hysteresis loss at the same crack growth velocity near the crack tip.[42] The values of J'' of the four composites plotted against temperature are presented in Figure 9. The CNTB-5 composite owned the lowest J'' by a dramatic margin at room temperature; this indicated the obviously highest hysteresis loss at the crack tip during the fatigue process.

When we combined the results of HED and J'', it showed that the CNTB-5 composite possessed the highest hysteresis loss by a dramatic margin, regardless of those in the bulk and at the crack tip. For untreated CNT-filled rubber composites, Cataldo *et al.*[48] attributed the relatively higher hysteresis under cyclic deformation to its relative weak interfacial interaction between the CNTs and rubber chains. For the CNTB-5 composite, the highest hysteresis resulted in marked heat generation and then elevated temperatures under dynamic conditions, all of which would accelerate the rupture of the molecular chain, suppress the strain-induced crystallization, and lead to the decrease in the fatigue crack growth resistance.

CONCLUSIONS

Synergetic effects between CNTBs and CB in NR composites were presented via marked enhancements in the mechanical properties, fracture, and fatigue crack growth resistance. Small

loadings of CNTBs greatly improved the fracture resistance of the CB/NR composites. The composite with 3-phr CNTBs exhibited the strongest resistance to fatigue crack growth. The increased strain-induced crystallization with the addition of the CNTBs accelerated the tendency toward crack deviation. The composite containing 5-phr CNTBs showed the weakest dynamic crack growth resistance, and the reason was the dramatically higher hysteresis loss of CNTB-5 compared to those of the other composites. Therefore, the optimum loading of CNTBs was the key to obtaining the synergetic effects between CNTBs and CB.

ACKNOWLEDGMENTS

The authors gratefully acknowledge the financial support of the National Natural Science Foundation of China (contract grant numbers 51333004 and 51221002) and the National Basic Research Program of China (973 Program 2011CB932603).

REFERENCES

1. Lake, G. J. *Rubber Chem. Technol.* **1995**, *68*, 435.
2. Lake, G. J. *Rubber Chem. Technol.* **2003**, *76*, 567.
3. Mars, W. V.; Fatemi, A. *Rubber Chem. Technol.* **2004**, *77*, 391.
4. Reincke, K.; Grellmann, W.; Heinrich, G. *Rubber Chem. Technol.* **2004**, *77*, 662.
5. Reincke, K.; Grellmann, W.; Lach, R.; Heinrich, G. *Macromol. Mater. Eng.* **2003**, *288*, 181.
6. Rivlin, R. S.; Thomas, A. G. *J. Polym. Sci.* **1953**, *10*, 291.
7. Thomas, A. G. *J. Polym. Sci.* **1958**, *31*, 467.
8. Young, D. G. *Rubber Chem. Technol.* **1990**, *63*, 567.
9. Lake, G. J.; Lindley, P. B. *J. Appl. Polym. Sci.* **1965**, *9*, 1233.
10. Rice, J. R.; Rosengren, G. F. *J. Mech. Phys. Solids* **1968**, *16*, 1.
11. Chow, C. L.; Wang, J.; Tse, P. N. *Tire Sci. Technol.* **1988**, *16*, 44.
12. Naït-Abdelaziz, M.; Zaïri, F.; Qu, Z.; Hamdi, A.; Aït Hocine, N. *Mech. Mater.* **2012**, *53*, 80.
13. Ramorino, G.; Agnelli, S.; De Santis, R.; Riccò, T. *Eng. Fract. Mech.* **2010**, *77*, 1527.
14. Agnelli, S.; Ramorino, G.; Passera, S.; Karger-Kocsis, J.; Riccò, T. *Express Polym. Lett.* **2012**, *6*, 581.
15. Dong, B.; Liu, C.; Wu, Y. P. *Polym. Test.* **2014**, *38*, 40.
16. Lorenz, H.; Fritzsche, J.; Das, A.; Stöckelhuber, K. W.; Jurk, R.; Heinrich, G.; Klüppel, M. *Compos. Sci. Technol.* **2009**, *69*, 2135.
17. Verge, P.; Peeterbroeck, S.; Bonnaud, L.; Dubois, P. *Compos. Sci. Technol.* **2010**, *70*, 1453.
18. Pedroni, L. G.; Araujo, J. R.; Felisberti, M. I.; Nogueira, A. F. *Compos. Sci. Technol.* **2012**, *72*, 1487.
19. Park, S. M.; Lim, Y. W.; Kim, C. H.; Kim, D. J.; Moon, W.-J.; Kim, J.-H.; Lee, J.-S.; Hong, C. K.; Seo, G. *J. Ind. Eng. Chem.* **2013**, *19*, 712.
20. Bokobza, L. *Rubber Chem. Technol.* **2013**, *86*, 423.
21. Ismail, H.; Ramly, A. F.; Othman, N. *Polym.-Plast. Technol.* **2011**, *50*, 660.
22. Fritzsche, J.; Lorenz, H.; Klüeppel, M. *Macromol. Mater. Eng.* **2009**, *294*, 551.
23. Kim, Y. A.; Hayashi, T.; Endo, M.; Gotoh, Y.; Wada, N.; Seiyama, J. *Scr. Mater.* **2006**, *54*, 31.
24. Rattanasom, N.; Prasertsri, S.; Ruangritnumchai, T. *Polym. Test.* **2009**, *28*, 8.
25. Agnelli, S.; Baldi, F.; Riccò, T. *Eng. Fract. Mech.* **2012**, *90*, 76.
26. Grellmann, W.; Reincke, K. Fracture Mechanics and Statistical Mechanics of Reinforced Elastomeric Blends; Springer: Berlin, **2013**; Chapter *6*, p 227.
27. Schubel, P. M.; Gdoutos, E. E.; Daniel, I. M. *Theor. Appl. Fract. Mech.* **2004**, *42*, 149.
28. Paris, P. C.; Erdogan, F. *J. Fluid. Eng.* **1963**, *85*, 528.
29. Liu, C.; Luo, Y. F.; Jia, Z. X.; Li, S. Q.; Guo, B. C.; Jia, D. M. *J. Macromol. Sci. Phys.* **2012**, *51*, 968.
30. Payne, A. R. *J. Appl. Polym. Sci.* **1962**, *6*, 57.
31. Kerchman, V.; Shaw, C. *Rubber Chem. Technol.* **2003**, *76*, 386.
32. Gent, A. N. Engineering with Rubber: How to Design Rubber Components; Hanser: Munich, **2001**; Chapter 5, p 122.
33. Furukawa, J.; Onouchi, Y.; Inagaki, S.; Okamoto, H. *Polym. Bull.* **1981**, *6*, 381.
34. Mark, J. E. *Polym. Eng. Sci.* **1979**, *19*, 254.
35. Bokobza, L. *Polymer* **2007**, *48*, 4907.
36. Nie, Y. J.; Huang, G. S.; Qu, L. L.; Wang, X. A.; Weng, G. S.; Wu, J. R. *Polymer* **2011**, *52*, 3234.
37. Mzabi, S.; Berghezan, D.; Roux, S.; Hild, F.; Creton, C. *J. Polym. Sci. Part B: Polym. Phys.* **2011**, *49*, 1518.
38. Morman, K. N., Jr.; Pan, T. Y. *Rubber Chem. Technol.* **1988**, *61*, 503.
39. Gent, A. N.; Razzaghi-Kashani, M.; Hamed, G. R. *Rubber Chem. Technol.* **2003**, *76*, 122.
40. Persson, B. N. J.; Brener, E. A. *Phys. Rev. E* **2005**, *71*, 036123.
41. Nie, Y. J.; Wang, B. Y.; Huang, G. S.; Qu, L. L.; Zhang, P.; Weng, G. S.; Wu, J. R. *J. Appl. Polym. Sci.* **2010**, *117*, 3441.
42. Rooj, S.; Das, A.; Morozov, I. A.; Stöckelhuber, K. W.; Stocek, R.; Heinrich, G. *Compos. Sci. Technol.* **2013**, *76*, 61.
43. Payne, A. R.; Whittaker, R. E. *J. Appl. Polym. Sci.* **1971**, *15*, 1941.
44. Lindley, P. B. *Int. J. Fract.* **1973**, *9*, 449.
45. Hamed, G. R. *Rubber Chem. Technol.* **1991**, *64*, 493.
46. Toki, S.; Fujimaki, T.; Okuyama, M. *Polymer* **2000**, *41*, 5423.
47. Wang, M. J. *Rubber Chem. Technol.* **1998**, *71*, 520.
48. Cataldo, F.; Ursini, O.; Angelini, G. *Fullerenes Nanotubes Carbon Nanostruct.* **2009**, *17*, 38.